Novel closed-loop control system for shunt active power filters: a comparative study with open-loop control

AGATA BIELECKA^{o1}, DANIEL WOJCIECHOWSKI^{o2}

¹Department of Measurement Science, Electronics and Control Faculty of Electrical Engineering, Silesian University of Technology 2A Akademicka Str., 44-100, Gliwice Poland

²Department of Power Electronics and Electrical Machines Faculty of Electrical and Control Engineering, Gdansk University of Technology 11/12 Gabriela Narutowicza Str, 80-233, Gdansk, Poland e-mail: a.bielecka@we.umg.edu.pl, daniel.wojciechowski@pg.edu.pl

Abstract: This paper proposes a novel closed-loop control system for a shunt active power filter, characterised by its high effectiveness in compensating for supply current harmonics. The proposed control algorithm is compared with the open-loop control, emphasising that no hardware modifications have been made. Thus, the differences in APF operation observed during the tests are solely due to the control algorithm. The research includes a multicriteria comparison of the two control systems under different operating conditions.

Key words: active power filter, closed-loop control, current harmonic compensation, open-loop control, power quality, predictive control

1. Introduction

In recent years, interest in power quality improvement has increased significantly because of growing deterioration of electric power quality delivery. It is mainly observed on account of numerous non-linear loads installed in the distribution networks and the development of renewable energy sources. It is primarily due to the distorted current forced by the devices with a non-linear voltage-current characteristic, which results in the voltage that deviates from its sinusoidal form. The distortion of the voltage waveform is more pronounced in weak grids because the supply current induces a voltage drop across the equivalent impedance of the power supply. The higher the impedance, the greater the voltage drop and voltage waveform deviation caused by that dependence. A shunt active power filter (APF) is considered the most effective and attractive tool for the problems of electric power quality, especially in networks with slowly varying, distorting loads. Not only does the APF compensate for the current harmonics, but also for reactive power and current unbalance.

In comparison to traditional passive filters (PF), the APF is distinguished by numerous advantages such as small size, parameter design accuracy, precise control, and robustness to resonance [1]. A shunt APF consists of a voltage source inverter (VSI) connected to the grid via a coupling circuit at the point of common coupling (PCC). The effectiveness of its operation depends mainly on two things: hardware (main circuit) and software (control). Aspects related to hardware encompass VSI DC voltage, switching frequency, non-linearities of the converter and the type of applied coupling circuit. Software issues, however, are related to the determination of the reference compensating current as well as the dynamics and accuracy of its generation, which results from the current controller. Another issue is the delays between measurements and control, which affects the accuracy of tracking the set current waveform.

Focusing on low-voltage distribution networks, a two-level VSI is sufficient and commonly applied. On the other hand, the topology of the coupling circuit can differ. It should pass the frequencies related to the compensated current harmonics and simultaneously suppress the high frequencies resulting from the pulse modulation of the converter. The simplest coupling circuit is the L-type filter. Nevertheless, for such a solution, a sufficiently high level of suppression of high-frequency current ripples can only be reached with inductance values that excessively limit the dynamics of the compensation current [2]. Despite this disadvantage, it has been widely utilised in both industry applications and academic research [1, 3–13]. Conversely, an LCL-type filter, whose dimensions are smaller, can overcome the drawbacks of the L-type filter and thus meet the requirements set for the coupling circuit. However, its implementation is more demanding due to the risk of resonance [2, 14–16].

There are two main shunt APF control strategies, each of which involves a multitude of methods and algorithms that determine the effectiveness of APF operation. The fundamental distinction between these strategies is whether the reference compensating current is determined using an additional, outer current control loop. If not, then the control is regarded as an open-loop (OL) system (Fig. 1) and the reference current is determined based on the load current signal, without the aforementioned, additional outer feedback.

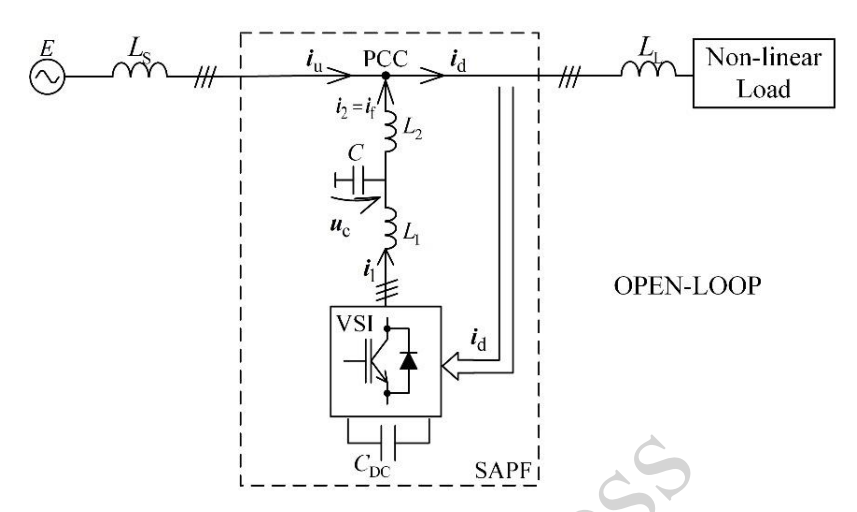


Fig. 1. Schematic diagram of APF open-loop concept

The primary characteristics of this control system, namely its notable resilience to variable operating conditions, its relatively brief transient state following a change in load current, and its minimal computational demands, have led to a considerable number of studies [2, 5, 6, 8, 11–13, 16, 17] devoted to this kind of control.

The other control, which constitutes a relatively novel approach, is closed-loop (CL) control (Fig. 2). This one uses an additional, outer current control loop from the supply current in order to extract and control current harmonics. It is worth noting that both methods (called OL and CL in the paper) use feedback from the state variables of the LCL coupling circuit and the DC voltage; thus, they are both control systems. The extant literature on this type of control is limited [1, 4, 9, 16]. In [1], the authors propose a method to derive the reference APF current using feedback from the supply current with a constant, arbitrarily set gain (P controller) for each harmonic. This approach results in nonzero errors in quasi-steady states. Paper [9] presents a multi-harmonic resonant controller for feedback from the supply current, which requires an additional supporting stabilization algorithm to address unwanted resonances. The CL control solution described in [16] operates in the frequency domain, but the current is obtained using the Fast Fourier Transform (FFT), which – under asynchronous sampling – introduces errors in harmonic amplitude estimation. An interesting approach is proposed in [4], where CL control is implemented using repetitive control. A limitation of the CL control methods presented in [1, 4], and [9] is that they assume an APF coupled to the grid via an inductor, which restricts their practical applicability due to the high level of PWM-related current ripples in the compensating current.

This paper proposes a novel CL control solution that is accurate, operates with an APF using an LCL coupling circuit, and achieves high compensation effectiveness compared to open-loop control. Moreover, it allows current harmonics to be reduced to specified levels, although it requires careful stability analysis [18–20].

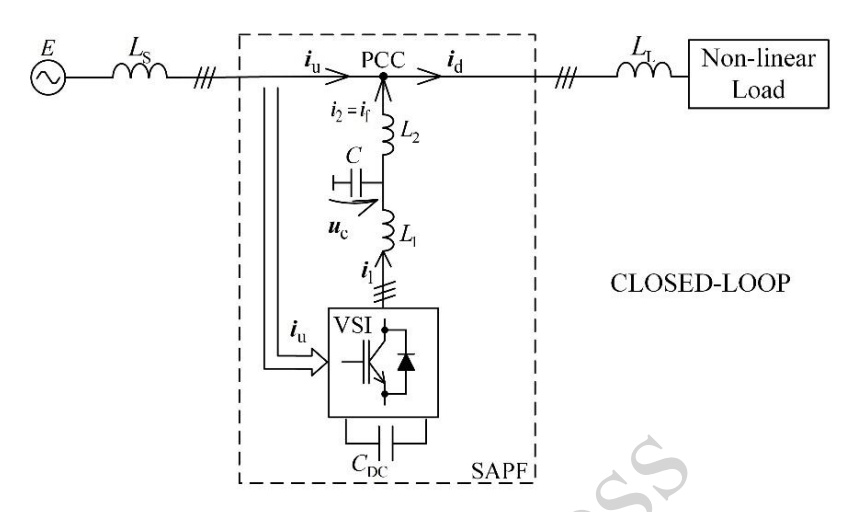


Fig. 2. Schematic diagram of closed-loop APF concept

A significant aspect of APF operation that is examined in this paper is its performance under varying load power. Despite the fact that this issue has been investigated by many researchers, most studies have focused on dynamic states [8, 14, 17]. While dynamics are imperative, it is equally crucial to evaluate the efficacy of current compensation when the APF is operating at partial power. In industrial applications, particularly those involving high-power APFs, custom designs are frequently adapted to specific system characteristics. This adaptation involves defining parameters such as power, which are then tailored to the system's unique specifications. For standard, non-customised designs, it is recommended that the power of the APF should be approximately 30% of the total load power; its negative effects on the supply network need to be mitigated. Nevertheless, APFs frequently operate at a fraction of their rated power capacity due to the fact that non-linear loads often function below their rated power capacity or do not operate concurrently. Consequently, the APF control system must provide effective current harmonic compensation over the entire operating range of the filter.

Another interesting issue raised in recent papers [15, 21] is the placement of APFs in electrical networks to achieve the desired THD of the supply current. However, this problem is more pronounced in open-loop control systems, as closed-loop control can more easily ensure current harmonic compensation at a well-defined point in the network.

This paper presents further research on the control system featured in [22–24]. Previous publications [22, 23] contain the simulation results without experimental verification. This paper focuses on comparing the open-loop and closed-loop control systems in terms of transient response time and current compensation effectiveness under varying levels of APF operating power relative to its rated power. The control systems were tested under different grid conditions, including stiff and weak grids. Both systems use predictive control to mitigate the negative effects of time delays introduced by the digital implementation of the control algorithm. Since the effectiveness of the compensation depends not only on the dynamics of the APF current but

also on its accurate generation, the tests also considered cases where the compensation current generation was altered by inverter non-linearities such as dead times.

2. APF circuit

The configuration of the shunt APF is depicted in Fig. 3. Its main circuit comprises a VSI connected to the PCC through an LCL coupling circuit. The APF operates as a controlled source of compensation current. This current is shaped via the coupling circuit using a PWM-controlled VSI, which functions as a three-phase AC voltage source. The purpose of the coupling circuit is to provide appropriate impedance within the compensation frequency range while offering the highest possible impedance at the PWM switching frequency and its higher harmonics. For this reason, a third-order LCL filter is employed. The analytical evaluation of the APF circuit and its control is based on a model of the power supply system, which includes an equivalent voltage source and Thevenin equivalent impedance composed of inductance L_s and resistance R_s . The load is modelled as a three-phase diode rectifier.

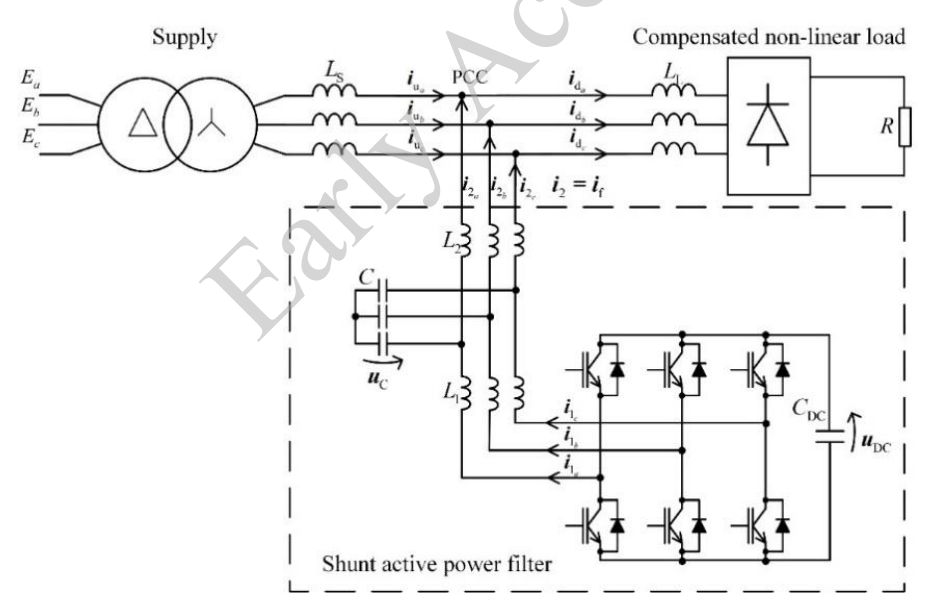


Fig. 3. Main circuit of a system with shunt APF

The mathematical representation of the APF circuit from Fig. 3 is developed using space vectors x, derived from the three-phase quantities x_a , x_b and x_c . The orthogonal components of these space vectors, x_α and x_β , are obtained through the Clarke transformation. The dynamic behaviour of the LCL coupling network is described by the following differential equations:

This paper has been accepted for publication in the AEE journal. This is the version, which has not been fully edited and content may change prior to final publication.

Citation information: DOI 10.24425/aee.2025.155960

$$L_1 \frac{di_1}{dt} = u_{VSI} - u_C, \quad C \frac{du_C}{dt} = i_1 - i_2, \quad L_2 \frac{di_2}{dt} = u_C - u_{PCC}.$$
 (1)

The resonant frequency of the LCL circuit results from the parallel configurations of L_1 and L_2 inductors along with capacitors. This is defined by the equation:

$$f_{\rm LCL} = \frac{\omega_{\rm LCL}}{2\pi} = \frac{1}{2\pi} \sqrt{\frac{L_1 + L_2}{L_1 L_2 C}}.$$
 (2)

The AC output voltage of the VSI, $u_{\rm VSI}$, is constrained by the DC-link voltage $u_{\rm DC}$. This constraint defines the feasible operating region for the VSI output voltage, as shown in Fig. 4. Within this region, time-averaged output voltages can be synthesized using PWM control. The circular boundary represents the onset of overmodulation and thus marks the limit of the VSI's linear operating range.

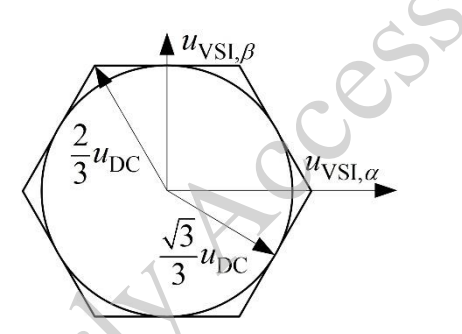


Fig. 4. The area of feasible voltage of the VSI

3. APF control

The task of the control system for a shunt APF, given a specific circuit structure and set of parameters, is to maximise the effectiveness of supply current compensation – regardless of the APF's operating conditions or operating point, in both steady-state and transient regimes. The performance of the control system depends on each of its functional blocks, with particular importance placed on the detection and control of the APF compensation current. As noted in the Introduction, most existing methods for determining the compensation current rely on open-loop calculations; however, closed-loop approaches appear to offer a greater potential.

The block diagram of the APF control system under investigation, capable of operating in both open-loop and closed-loop configurations, is shown in Fig. 5. The signal processing carried out by the control algorithms is based on a complex signal representation of the three-phase quantities. These signals are derived by projecting space vectors from the orthogonal α , β plane onto the corresponding complex plane.

This paper has been accepted for publication in the AEE journal. This is the version, which has not been fully edited and content may change prior to final publication.

Citation information: DOI 10.24425/aee.2025.155960

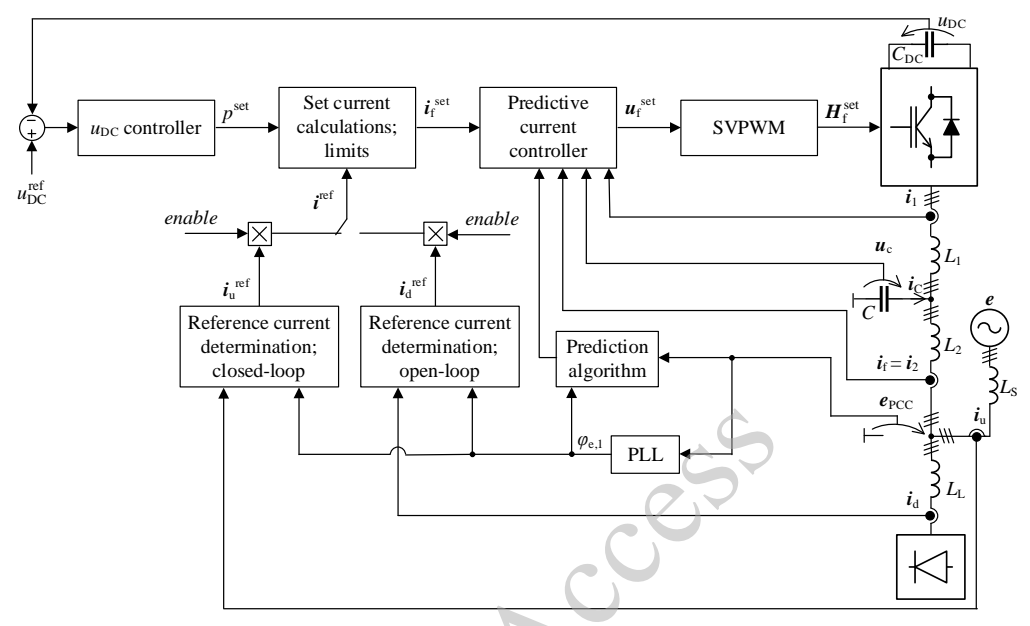


Fig. 5. Block diagram of the universal, open-loop and closed-loop APF control system

Each functional block of the control system is designed to maximise the effectiveness of the APF. The control command – specifically, the reference voltage for Space Vector Pulse-Width Modulation (SVPWM) – is computed at a fixed sampling interval T_s . Both the OL and CL configurations utilise a shared current controller. This controller is predictive and model-based, delivering a near-deadbeat dynamic response, damping the resonance of the LCL coupling circuit and compensating for feedback-to-control delays. The control algorithm is defined by the following set of difference equations presented originally in [22]:

$$\widehat{\boldsymbol{u}}_{C}(n-1) = T_{S} \frac{i_{1}(n-1) - i_{2}(n-1)}{C} + \boldsymbol{u}_{C}(n-2), \tag{3}$$

$$\hat{\mathbf{i}}_{1}(n) = T_{S} \frac{u_{\text{VSI}}^{\text{set,lim}}(n-1) - \hat{\mathbf{u}}_{C}(n-1)}{L_{1}} + \mathbf{i}_{1}(n-1), \tag{4}$$

$$\hat{\mathbf{i}}_{2}(n) = T_{S} \frac{\hat{\mathbf{u}}_{C}(n-1) - \tilde{\mathbf{e}}_{PCC}(n-1)}{L_{2}} + \hat{\mathbf{i}}_{2}(n-1), \tag{5}$$

$$\widehat{\boldsymbol{u}}_{\mathcal{C}}(n) = T_{\mathcal{S}} \frac{\widehat{\boldsymbol{\iota}}_{1}(n) - \widehat{\boldsymbol{\iota}}_{2}(n)}{c} + \widehat{\boldsymbol{u}}_{\mathcal{C}}(n-1), \tag{6}$$

$$\hat{\boldsymbol{u}}_{\mathcal{C}}(n+1) = L_2 \frac{i_2^{\text{set}}(n+2) - i_2^{\text{set}}(n+1)}{T_{\mathcal{S}}} + \tilde{\boldsymbol{e}}_{PCC}(n+1), \tag{7}$$

$$\hat{\mathbf{i}}_1(n+1) = C \frac{\hat{\mathbf{u}}_C(n+1) - \hat{\mathbf{u}}_C(n)}{T_S} + \hat{\mathbf{i}}_2^{\text{set}}(n+1), \tag{8}$$

$$\hat{\mathbf{i}}_{1}^{\text{lim}}(n+1) = \text{sign}\{\hat{\mathbf{i}}_{1}(n+1)\} \cdot \min\{|\hat{\mathbf{i}}_{1}(n+1)|, I_{1}^{\text{max}}\},\tag{9}$$

$$\boldsymbol{u}_{\text{VSI}}^{\text{set}}(n) = L_1 \frac{\hat{\imath}_1^{\text{lim}}(n+1) - \hat{\imath}_1(n)}{T_S} + \widehat{\boldsymbol{u}}_C(n), \tag{10}$$

where predicted quantities are denoted with a hat, calculated values with a wide hat, and the predicted PCC voltage e_{PCC} with a tilde. In the current controller, the predicted voltage at the PCC – used in Eqs. (5) and (7) – is estimated under the assumption of periodicity, employing a circular buffer for this purpose.

What distinguishes the OL and CL configurations is the method used to determine the compensation current. In the OL configuration, a well-established approach based on the instantaneous power theory is applied. This broadband method, when anchored to the fundamental positive-sequence component of the supply voltage, ensures that the computed reference current remains unaffected by voltage quality.

In the CL configuration, a dedicated algorithm is proposed for the selective control of individual harmonics within the reference compensation current. The block diagram illustrating the extraction of specific current harmonics is presented in Fig. 6.

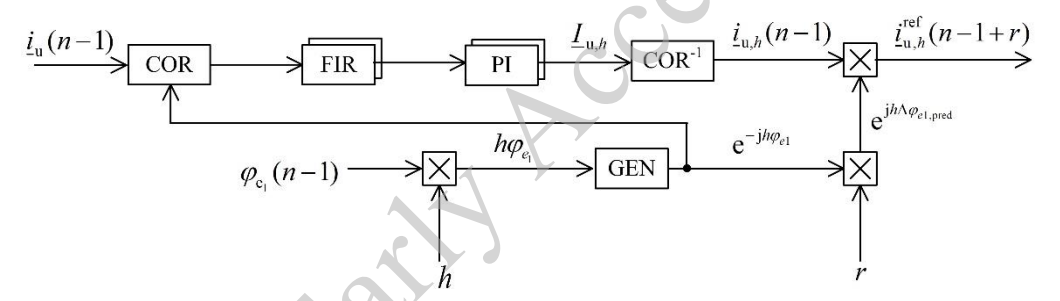


Fig. 6. Block diagram of the particular, upstream current harmonic control in the closed-loop APF control system

The input to this algorithm is the feedback signal from the supply (upstream) current i_u , which is to be compensated. The complex time-domain representation of this current is transformed into the frequency domain and expressed as a set of complex amplitudes corresponding to selected harmonics. This is achieved by cross-correlating the complex basis functions $e^{-jh\varphi_{e,1}}$ of the desired harmonics with the input signal. To obtain this basis signal, the actual angle of the grid voltage $\varphi_{e,1}$ is multiplied by the harmonic order h, and then cosine (Re) and sine (Im) components are generated in the block marked with GEN. The cross-correlation is realized in the COR block according to the following equation:

$$\underline{I}_{u,h} = \overline{\underline{i}_u e^{-jh\varphi_{e,1}}},\tag{11}$$

where the dash denotes low-pass filtering. The real and imaginary parts of the h^{th} complex amplitude are expressed by the following equations:

$$\operatorname{Re}(\underline{I}_{u,h}) = \underline{\underline{i}_{u} \cdot \cos(h\varphi_{e,1}) + \underline{i}_{u} \cdot \sin(h\varphi_{e,1})}, \tag{12}$$

$$\operatorname{Im}(\underline{l}_{u,h}) = \overline{\underline{l}_{u} \cdot \cos(h\varphi_{e,1}) - \underline{l}_{u} \cdot \sin(h\varphi_{e,1})}. \tag{13}$$

The low-pass filtering present in Eqs. (11), (12), and (13) is implemented via a Finite Impulse Response (FIR) moving average filter, which offers the fastest possible step response. This property is crucial for minimising the response time of the CL-controlled APF under dynamic conditions, such as sudden changes in the compensated loads. The calculated complex amplitudes $\underline{I}_{u,h}$ are controlled to zero using a set of two PI controllers for complex amplitude (real and imaginary parts) of a single complex harmonic. This approach enables selective control of specific current harmonics, which can be adjusted to any desired level by assigning a non-zero reference value. To control each current harmonic, four PI controllers have to be employed in total: two for the positive-sequence harmonic component and two for the negative-sequence component of the h^{th} -order harmonic. The outputs of these PI controllers represent the complex amplitudes of the APF reference compensation current. These outputs are subsequently predicted through vector rotation, expressed as:

$$\Delta \varphi_{e,1,h,\text{pred}} = \Delta \varphi_{e,1} \cdot h \cdot r, \tag{14}$$

where $\Delta \varphi_{e,1}$ denotes the angle increment of the fundamental frequency of the supply voltage over the sampling interval T_s , as determined by the PLL, and r represents the prediction horizon. The necessary predicted samples of the reference APF current are computed using an IDFT-based method, in which the actual instantaneous angle of the fundamental frequency at the PCC is utilised:

$$i_{f,h}^{\text{ref}} = \underline{I}_{f,h} e^{jh\varphi_{e,1,h,\text{pred}}} e^{j\Delta\varphi_{e,1,h,\text{pred}}}.$$
 (15)

Finally, all the individually determined compensation reference current harmonics are superimposed to construct the final reference current to be generated by the APF.

It is important to note that the block diagram presented in Fig. 6 corresponds to the control of a single component (positive or negative) or a specific current harmonic to be selectively compensated. Therefore, two such algorithm sets are required to compensate for a single current harmonic, covering both its symmetrical and asymmetrical components.

4. Experimental results

The theoretical assumptions were experimentally verified using a 4 kVA shunt APF. The implemented APF featured a three-leg VSI connected to the grid via an LCL coupling circuit. Measurements were carried out using a ZES Zimmer LMG 670 power quality analyser and a Tektronix MDO 4104B oscilloscope. The laboratory setup is illustrated in Fig. 7. The tests were conducted under two grid conditions: a stiff grid, characterised by $L_S = 48 \mu H$; $k_{sc,rel} = 597$ and a weak grid, with $L_S = 1.47 \mu H$, $R_S = 0.46 \mu C$; $k_{sc,rel} = 14$, where $k_{sc,rel}$ represents the short-circuit power factor relative to the rated power of the nonlinear load. Unless stated otherwise in the text,

all measurements were conducted with the filter operating at its nominal power. The detailed parameters of the shunt APF laboratory setup are listed in Table 1.

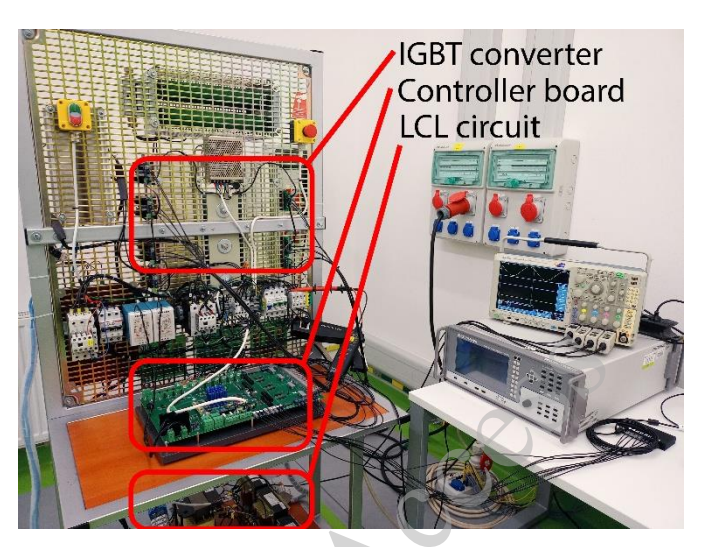


Fig. 7. The laboratory setup with APF of rated power 4 kVA

Table 1. Parameters of the shunt APF used in the experimental tests

Parameter name	Symbol	Value	Unit
Effective grid line-to-line voltage	E	3 × 400	V
Grid voltage frequency	f_e	50	Hz
APF rated power	$S_{ m APF}$	4	kVA
DC voltage of the VSI	$U_{ m DC}$	750	V
SVPWM frequency (f _{PWM} = 0.5f _s)	fрwм	12.5	kHz
Coupling circuit inverter-side inductance	L_1	2.75	mH
Coupling circuit grid-side inductance	L_2	1.0	mH
Coupling circuit capacitance	С	3.0	μF
Capacitance in the DC circuit of the VSI	$C_{ m DC}$	1.05	mF
Dead time	$\mathrm{d}T$	2.5	μs
Closed-loop PI controllers proportional gain	K_p	0.02	-
Closed-loop PI controllers integral gain	Kı	10.0	-
Prediction horizon	r	3	-
Order of FIR filters	N	500	-

All tests were conducted using the same hardware configuration to ensure consistent operating conditions and to isolate the evaluation of the proposed control systems' effectiveness in compensating for current distortion. The two control strategies compared are the open-loop (OL) and closed-loop (CL). In OL control mode, broadband harmonic compensation has been used. For CL current control, the harmonics of order $h = 6n \pm 1$ ($n \in \mathbb{N}$) from h = 5 up to h = 49 have been selectively compensated. That means, 16 positive sequence and 16 negative sequence harmonics -32 harmonics in total. The distorted load current was produced by a three-phase diode rectifier with a resistive load on the DC side.

The transient waveforms of the PCC voltage, as well as the upstream, downstream, and active filter currents following the activation (step from 0 to 100% power) of the nonlinear load, are presented in Figs. 8 and 9. Such a transient is most demanding for the APF control system – regardless of its control. These results indicate that the transient duration in the CL-controlled system is significantly longer than in the OL-controlled system. In the CL case, the waveforms stabilise after approximately four fundamental periods, whereas in the OL configuration, stability is achieved after roughly one period. This implies that the OL strategy responds more rapidly to load disturbances, while the CL strategy exhibits slower adaptation due to the additional external current control loop.

The detailed relationship between response time and the effectiveness of current harmonic compensation, quantified by the THD of the upstream current (THD $_{iu}$), is illustrated in Figs. 10 and 11. These plots depict the control-system behaviour under both considered grid conditions. The results demonstrate that the CL strategy requires more than ten times longer to reach a steady state compared to the OL strategy. However, it achieves a THD $_{iu}$ level approximately 1.5 to 2 times lower than that of the OL configuration.

The frequency spectra of upstream current harmonic amplitudes in the case of no harmonic compensation in both stiff and weak grid conditions are illustrated in Fig. 12. Then, a comparison of the harmonic amplitudes of the upstream current after compensation performed in closed-loop and open-loop control systems is provided in Figs. 13 and 14. These frequency spectra were captured under steady-state conditions for all test cases, and the corresponding THD_{iu} values are indicated in the figures.

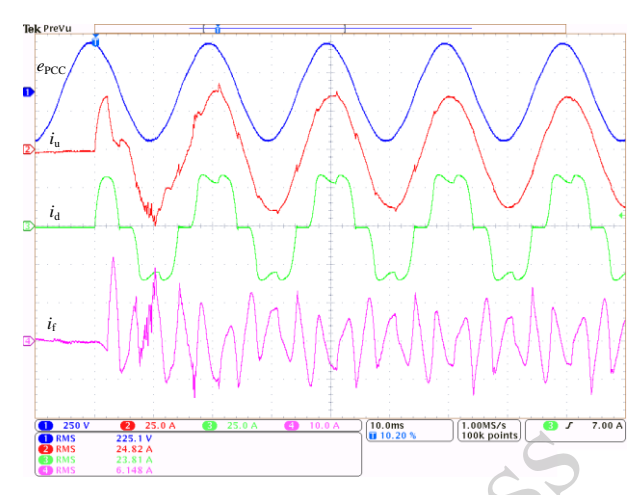


Fig. 8. Transient waveforms of e_{PCC} , i_u , i_d , after the load is switched on, obtained in open-loop control system under stiff network conditions



Fig. 9. Transient waveforms of e_{PCC} , i_u , i_d , after the load is switched on, obtained in closed-loop control system under stiff network conditions

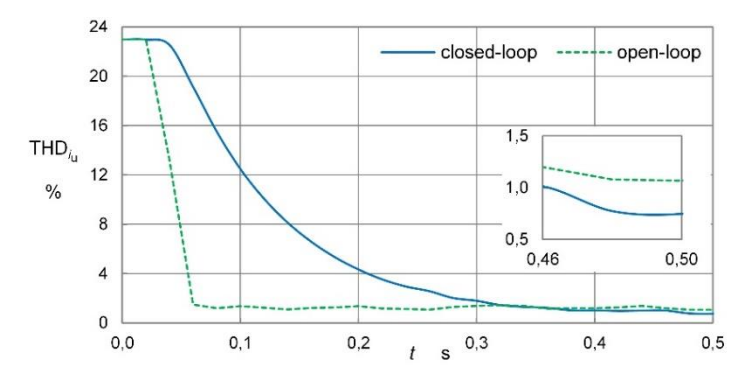


Fig. 10. The value of the THD_{iu} factor as a function of time obtained in open and closed loop control systems under stiff network conditions

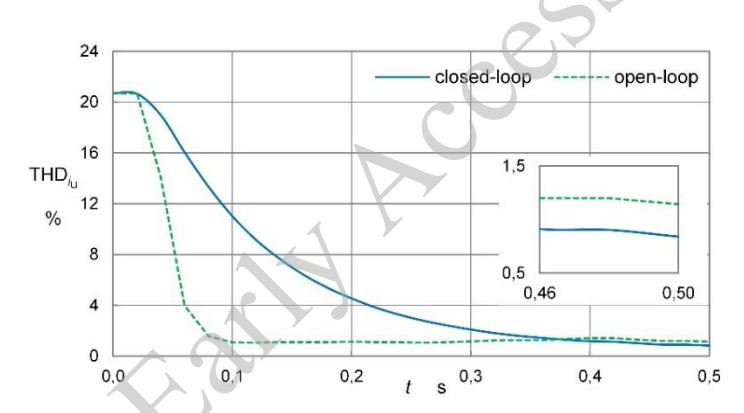


Fig. 11. The value of the THD_{iii} factor as a function of time obtained in open and closed loop control systems under weak network conditions

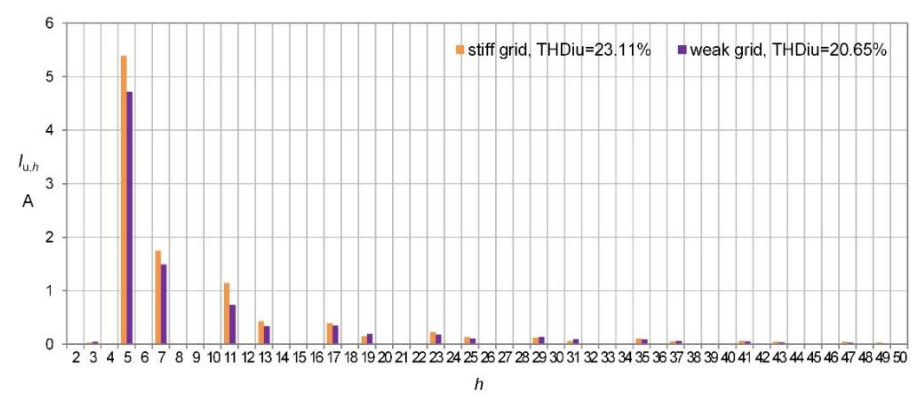


Fig. 12. The frequency spectra of the upstream current when no compensation is realised in the system

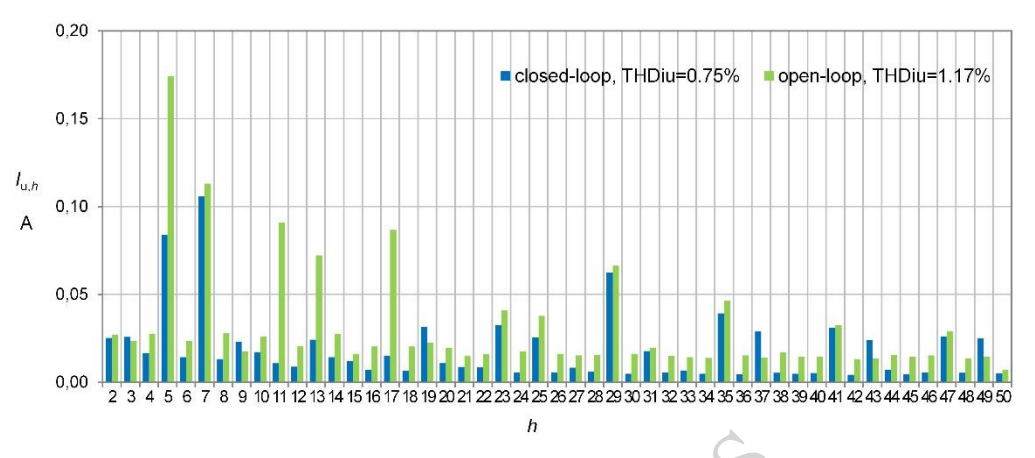


Fig. 13. The frequency spectra of the upstream current obtained for the current harmonic compensation carried out in the open and closed loop control systems in the stiff network conditions

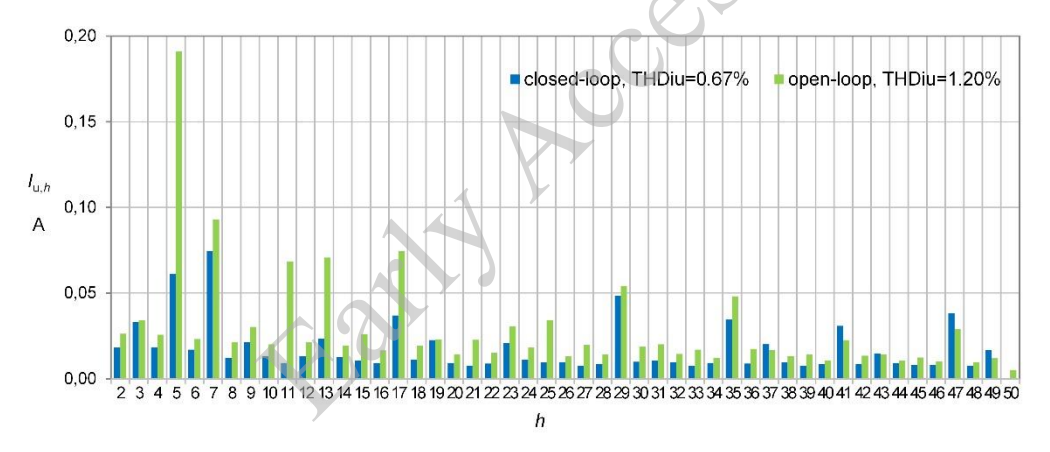


Fig. 14. The frequency spectra of the upstream current obtained for the current harmonic compensation carried out in the open and closed loop control systems in the weak network conditions

The obtained results confirm that closed-loop control provides a significantly higher level of current harmonic compensation than is achievable with open-loop control. As previously emphasised, a particularly important issue – often overlooked – is the compensation effectiveness, when the active power filter operates at a fraction of its rated power, a scenario frequently encountered in industrial applications. The relationship between the compensation level, expressed by the THD_{iu} of the upstream current, and the APF operating power is presented in Figs. 15 and 16. The results show a clear trend: as the APF operating power decreases, the THD_{iu} increases for both control strategies, regardless of the grid conditions. This is attributed to the fact that the proportion of harmonic content in the filter current becomes more significant at lower current amplitudes and consequently lower APF power levels.

Errors in the generated APF current – i.e., deviations between the reference and actual current – reduce the effectiveness of compensation. This issue is particularly evident in the OL control configuration, where THD_{iu} values in the range of 4.5% to 5% were observed – approximately twice as high as those achieved using CL control, irrespective of the grid stiffness.

One key contributor to these current-generation errors is inverter voltage inaccuracy, largely due to its inherent nonlinearities, such as dead time effects. Figure 17 illustrates the compensation effectiveness as a function of APF operating power in the presence of dead times. The most unfavourable scenario – low APF power combined with dead time distortion – yields the highest error levels in the filter current.

The THD $_{iu}$ curve for the OL control strategy in this condition shows substantially higher values compared to the case where dead time compensation [26] is implemented (Fig. 15). In some cases, the THD $_{iu}$ values differ by a factor of up to four for corresponding operating power levels.

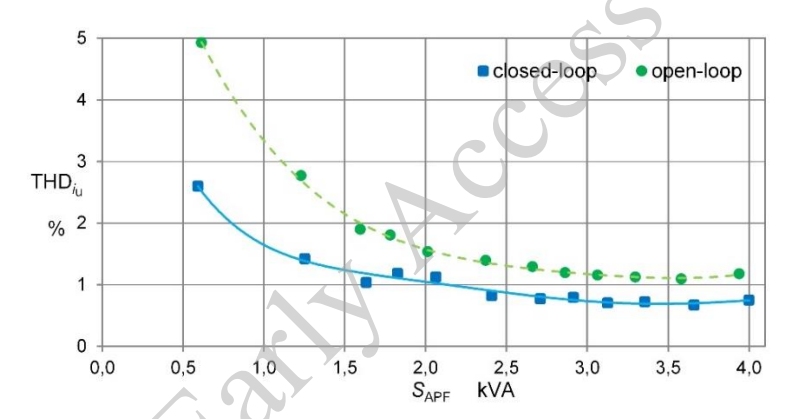


Fig. 15. THD_{iu} factor as a function of APF operating power obtained in open-loop and closed-loop control systems under stiff network conditions

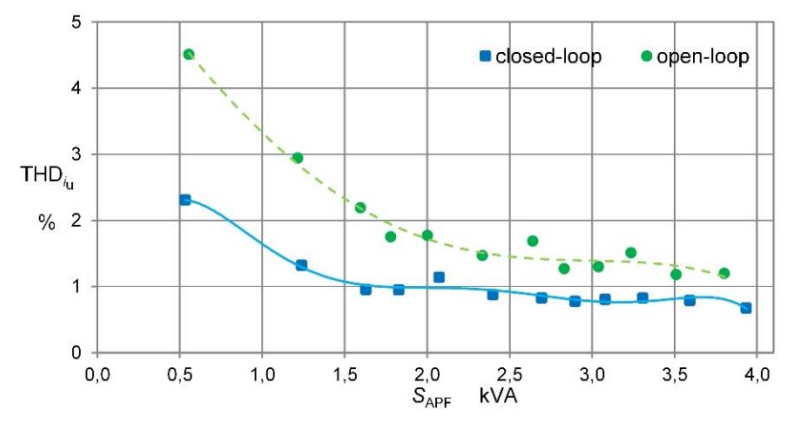


Fig. 16. THD_{iu} factor as a function of APF operating power obtained in open-loop and closed-loop control systems under weak network conditions

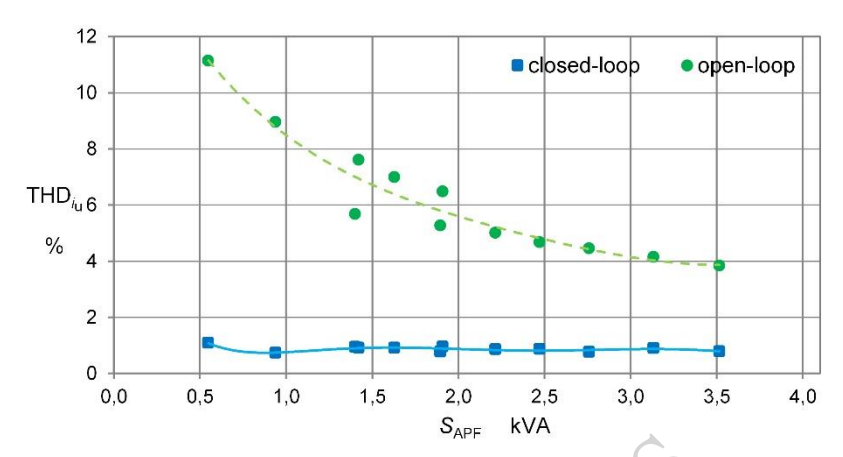


Fig. 17. THD_{iu} factor as a function of APF operating power, obtained in open-loop and closed-loop control systems under stiff network conditions with uncompensated dead times

These findings confirm that inaccurate voltage generation by the inverter – primarily due to dead time effects – has a significant impact on the shape of the generated current waveform, and thus on the overall effectiveness of APF operation. Nevertheless, the THD_{iu} values achieved with the CL control system remain substantially lower, with a maximum value of just 1.08%, which is more than ten times lower than that observed in the OL configuration.

This demonstrates that the proposed CL control strategy offers a notable additional benefit: it effectively addresses the complex issue of dead time compensation. Moreover, the total current harmonic distortion observed under CL control remains relatively consistent across the entire range of APF operating power considered, further confirming its robustness and effectiveness.

5. Conclusion

The findings presented in this study confirm the effectiveness of the proposed novel closed-loop control algorithm for shunt active power filters, demonstrating superior compensation of supply current components compared to the open-loop control strategy. This advantage is particularly pronounced when the APF operates at a fraction of its rated power – a condition often overlooked in academic research but frequently encountered in industrial applications.

In addition to providing enhanced harmonic compensation, the CL control system also exhibits strong robustness against errors in voltage generation caused by inverter nonlinearities, such as dead times. The results clearly indicate that significant improvements in current compensation performance can be achieved solely through control-algorithm enhancement, without incurring any additional hardware costs.

References

- [1] Yi H., Zhuo F., Zhang Y., Li Y., Zhang W., Chen W., Liu J., A source-current-detected shunt active power filter control scheme based on vector resonant controller, IEEE Transaction on Industry Applications, vol. 50, no. 3, pp. 1953–1965 (2014), DOI: 10.1109/TIA.2013.2289956.
- [2] Hu J.-G., Shi Y., Cheng G.-Y., A state-space approach to the integration of detection and control for shunt active power filter, 35th Chinese Control Conference, pp. 8660–8665 (2016), DOI: 10.1109/chicc.2016.7554739.
- [3] Ibanez-Hidalgo I., Cuzmar R.H., Sanchez-Ruiz A., Perez-Basante A., Zubizarreta A., Ceballos S., Aguilera R.P., *Enhanced PI control based SHC-PWM strategy for active power filters*, IEEE Open Journal of the Industrial Electronics Society, vol. 5, pp. 1174–1189 (2024), DOI: 10.1109/OJIES.2024.3483293.
- [4] Mattavelli P., Marafao F.P., Repetitive-based control for selective harmonic compensation in active power filters, IEEE Transactions on Industrial Electronics, vol. 51, pp. 1018–1024 (2004), DOI: 10.1109/TIE.2004.834961.
- [5] Li Y., Yi H., Zhuo F., Jiang X., Analysis and stabilization of APF systems considering dynamic of nonlinear loads, IEEE Transactions on Power Electronics, vol. 39, no. 1, pp. 409–423 (2024), DOI: 10.1109/TPEL.2023.3324650.
- [6] Lin H., Guo X., Chen D., Wu S., Chen G., A frequency adaptive repetitive control for active power filter with 380v/75a sic-inverter, IEEE Transactions on Industry Applications, vol. 58, no. 4, pp. 5469–5479 (2022), DOI: 10.1109/TIA.2022.3176848.
- [7] Gao C., He S., Cui B., Zhang B., Ming L., Leung K.N., Loh P.C., *Quantization effects on digital-PR-controlled active power filter*, IEEE Journal of Emerging and Selected Topics in Power Electronics, vol. 11, no. 6, pp. 5785–5797 (2023), DOI: 10.1109/JESTPE.2023.3313814.
- [8] Pichan M., Seyyedhosseini M., Hafezi H., *A new deadbeat based direct power control of shunt active power filter with digital implementation delay compensation*, IEEE Access, vol. 10, pp. 72866–72878 (2022), DOI: 10.1109/ACCESS.2022.3188685.
- [9] Li Y., Yi H., Zhuo F., Jiang X., Harmonic oscillation and stabilization strategy of source-current-detected shunt APF considering interaction with nonlinear load and grid impedance, IEEE Journal of Emerging and Selected Topics in Power Electronics, vol. 12, no. 1, pp. 420–430 (2024), DOI: 10.1109/JESTPE.2023.3329171.
- [10] Chen H., Liu H., Xing Y., Hu H., Enhanced DFT-based controller for selective harmonic compensation in active power filters, IEEE Transactions on Power Electronics, vol. 34, no. 8, pp. 8017–8030 (2019), DOI: 10.1109/TPEL.2018.2877848.
- [11] Urrea-Quintero J.-H., Munoz-Galeano N., Lopez-Lezama J.M., Robust control of shunt active power filters: A dynamical model-based approach with verified controllability, Energies, vol. 13, no. 23 (2020), DOI: 10.3390/en13236253.
- [12] Rahman S., Cervantes R., Khan I.A., Iqbal A., Ayob S., Active power filtering solution for improving power quality in cold ironed electric ships, IEEE Conference on Energy Conversion (2021), DOI: 10.1109/CENCON51869.2021.9627303.
- [13] Zhang Y., Dai K., Chen X., Kang Y., Dai Z., Stability analysis of SAPF by viewing DFT as cluster of BPF for selective harmonic suppression and resonance damping, IEEE Transactions on Industry Applications, vol. 55, no. 2, pp. 1598–1607 (2019), DOI: 10.1109/TIA.2018.2872649.
- [14] Yang L., Yang J., Gao M., Chen Y., Zhang X., A systematic approach via IIR filters for enhancing the robustness of LCL-type shunt active power filters to grid impedance, IEEE Transactions on Industry Applications, vol. 56, no. 5, pp. 5095–5107 (2020), DOI: 10.1109/TIA.2020.2999273.
- [15] Yang Z., Yi H., Zhuo F., Yin X., Wei W., Zhang Y., Zhang H., Wang Q., A system-level harmonic control method based on multi bus voltage detected APF without exact phase synchronization, IEEE Journal of Emerging and Selected Topics in Power Electronics, vol. 11, no. 3, pp. 2618–2631 (2023), DOI: 10.1109/JESTPE.2023.3267021.

- [16] Mariethoz S., Rufer A., Open loop and closed loop spectral frequency active filtering, IEEE Transactions on Power Electronics, vol. 17, no. 4, pp. 564–573 (2002), DOI: 10.1109/TPEL.2002.800973.
- [17] Karbasforooshan M.-S., Monfared M., *Adaptive predictive deadbeat current control of single-phase multi-tuned shunt hybrid active power filters*, IEEE Transactions on Power Delivery, vol. 39, no. 1, pp. 446–454 (2024), DOI: 10.1109/TPWRD.2023.3262662.
- [18] Yang L., Yang J., Gao M., Watson A., Wheeler P., Current control of LCL-type shunt APFs: Damping characteristics, stability analysis, and robust design against grid impedance variation, IEEE Journal of Emerging and Selected Topics in Power Electronics, vol. 9, no. 4, pp. 5026–5042 (2021), DOI: 10.1109/JESTPE.2020.3017551.
- [19] Briz F., Garcia P., Degner M.W., Diaz-Reigosa D., Guerrero J.M., Dynamic behaviour of current controllers for selective harmonic compensation in three-phase active power filters, IEEE Transactions on Industry Applications, vol. 49, no. 3, pp. 1411–1420 (2013), DOI: 10.1109/TIA.2013.2253537.
- [20] Bielecka A., Wojciechowski D., Stability analysis of shunt active power filter with predictive closed-loop control of supply current, Energies, vol. 14, no. 8, pp. 1–17 (2021), DOI: 10.3390/en14082208.
- [21] Bula D., Grabowski D., Lewandowski M., Maciazek M., Piwowar A., Software solution for modeling, sizing, and allocation of active power filters in distribution networks, Energies, vol. 14, no. 1 (2021), DOI: 10.3390/en14082208.
- [22] Bielecka A., Wojciechowski D., *Predictive control of a parallel active filter with feedback from the supply current*, Przegląd Elektrotechniczny, vol. 95, no. 6, pp. 128–132 (2019), DOI: 10.15199/48.2019.06.23.
- [23] Bielecka A., Wojciechowski D., Compensation of supply current harmonics, reactive power, and unbalanced load current balance in the closed-loop control of a shunt active power filter, Scientific Papers of the Maritime University of Szczecin, vol. 133, no. 61, pp. 9–16 (2020), DOI: 123456789/2609.
- [24] Bielecka A., Wojciechowski D., Parallel active filter controlled with feedback from the supply current laboratory tests, Przegląd Elektrotechniczny, vol. 99, no. 9, pp. 245–257 (2023).
- [25] Wojciechowski D., *Unified LCL circuit for modular active power filter*, COMPEL The International Journal for Computation and Mathematics in Electrical and Electronic Engineering, vol. 31, no. 6, pp. 1985–1997 (2012), DOI: 10.13199/48.2023.05.30.
- [26] Szwarc K.J., Cichowski A., Nieznanski J., Szczepankowski P., Modeling the effect of parasitic capacitances on the dead-time distortion in multilevel NPC inverters, IEEE International Symposium on Industrial Electronics, Gdansk, Poland, pp. 1869–1874 (2011), DOI: 10.1109/ISIE.2011.5984442.